

Davydov Splitting in the Optical Absorption Spectra of the Cr^{+3} 2E State in Some Rare-Earth Orthochromites*

R. S. Meltzer

Department of Physics, The Johns Hopkins University, Baltimore, Maryland 21218

(Received 30 April 1970)

We report here the R -line optical absorption spectra of Cr^{+3} in the rare-earth orthochromites ErCrO_3 , HoCrO_3 , and YCrO_3 as a function of an applied magnetic field. All three materials exhibit Davydov splittings. Their polarized spectra are found to be dissimilar. It is shown that these differences arise from the different types of spin structures which these materials exhibit in their magnetically ordered phases, and that from the polarization characteristics the magnetic factor group may be determined. ErCrO_3 is found to undergo a spin reorientation at 9°K . The $\vec{k}=0$ exciton problem is solved for the different spin structures and the transfer-of-energy matrix elements responsible for the Davydov splittings are determined. They are 5 to 100 times smaller than those of the corresponding excited state of Cr^{+3} in Cr_2O_3 . The differences are shown to arise from a combination of the different crystal structures of the two materials and the spin selection rules on the transfer-of-energy matrix elements.

I. INTRODUCTION

In order to interpret the optical spectrum of magnetic insulator crystals it has been necessary, in only a few cases, to consider the exciton nature of the electronically excited states. Some examples of these are (1) line shape of the magnon sidebands observed in several antiferromagnets,¹ (2) line shape of transitions from the first thermally populated spin excitation of the ferromagnet GdCl_3 ,² and (3) Davydov splitting in the two antiferromagnets Cr_2O_3 ^{3,4} and YCrO_3 .⁵ The exciton description becomes necessary when the electronic excitation can transfer rapidly among the ions of the crystal. In this paper we consider the Davydov splitting of the series of isostructural compounds $R\text{CrO}_3$ (R denotes rare earth).

In both Cr_2O_3 and YCrO_3 the Davydov splitting is observed in the transitions corresponding to the ruby R lines. We report here a study of the corresponding transitions in the two related rare-earth orthochromite crystals ErCrO_3 and HoCrO_3 and some new information on the YCrO_3 spectrum. All three materials exhibit Davydov splittings with transition selection rules to the Davydov components characterized by the magnetic symmetry of the crystal.

In Sec. IIA the construction of the Frenkel excitons necessary to describe the excited states of insulating crystals is briefly reviewed with emphasis on the relationship of the transfer-of-energy interaction to that of interionic interactions in general. In Sec. IIB the properties of the $R\text{CrO}_3$ crystals and the relevant single-ion states are described. The exciton theory is applied to $R\text{CrO}_3$ in Sec. IIC. The energy matrices for the $\vec{k}=0$ excitons are derived for the three types of magnetic

order which are compatible with the crystal structure and which preserve the paramagnetic unit cell, and include the effect of an external magnetic field along the antiferromagnetic axis. From the solutions, the selection rules and relative intensities of the exciton transitions are computed. They are shown to be different for each of the magnetic symmetries considered. The theory is compared to the observed spectra as a function of magnetic field in Sec. III. From this comparison we determine the appropriate magnetic factor group for the several $R\text{CrO}_3$'s and the corresponding transfer-of-energy matrix elements between a Cr^{+3} ion in the 2E excited state and its three translationally inequivalent types of neighbors in the ground state. For ErCrO_3 they are found to be highly sensitive to the type of magnetic order. Finally, in Sec. IV the transfer-of-energy matrix elements are compared to the previously determined values for Cr_2O_3 and are found to be 5 to 100 times smaller. The differences are shown to arise from dissimilar superexchange paths in the two materials.

II. THEORY

In this section we wish to review the position of transfer-of-energy in the framework of interionic interactions, to discuss how the transfer-of-energy leads to an exciton description of the excited states of weakly interacting magnetic ions in ionic insulators, and to consider the specific problem of excitons for the different magnetic spin configurations of $R\text{CrO}_3$. In the description which follows we treat the excitations as Frenkel excitons, as Loudon has shown this to be the proper description for magnetic insulators.⁶

A. Interionic Interaction and Description of Excitons

To begin with, an ionic crystal of N unit cells is constructed, each consisting of p molecular units. The Hamiltonian for the crystal is

$$\mathcal{H} = \mathcal{H}_0 + \sum_{n \geq m} \sum_{i \geq j}' \mathcal{H}_{ni, mj}, \quad (2.1)$$

$$\mathcal{H}_{ni, mj} = \sum_{s > t} \frac{e^2}{|\vec{r}_s - \vec{r}_t|},$$

where \mathcal{H}_0 is the free-ion Hamiltonian and \vec{r}_s and \vec{r}_t describe the positions of the two electrons. The prime on the summation indicates that when $n = m$, the $i = j$ term is excluded. The summation $s > t$ includes all pairs of electrons, one on the i th ion of the n th unit cell and one on ion mj . Initially, the two states of the crystal are defined as products of the free-ion eigenstates of \mathcal{H}_0 . The ground crystal state is

$$|F^0\rangle = |f_{11}^0 f_{12}^0 \cdots f_{1p}^0 \cdots f_{ni}^0 \cdots f_{Np}^0\rangle, \quad (2.2)$$

while that in which ion ni is excited from the ground state f^0 to f^w is

$$|F_{ni}^w\rangle = |f_{11}^0 f_{12}^0 \cdots f_{1p}^0 \cdots f_{ni}^w \cdots f_{Np}^0\rangle. \quad (2.3)$$

There are Np degenerate crystal states for each of the free-ion excited states. States of the crystal in which more than one ion are excited will not concern us here. The eigenstates of the crystal under \mathcal{H} can be found by solving the matrix in the representation defined above.

Consider the matrix of \mathcal{H} in this basis. The matrix elements can be grouped into two classes: those which do not transfer energy among the ions, such as $\langle F_{ni}^w | \mathcal{H} | F_{ni}^w \rangle$ called "static" matrix elements, and the transfer-of-energy matrix elements $\langle F_{ni}^w | \mathcal{H} | F_{mj}^w \rangle$. Since \mathcal{H} contains a two-electron interaction, both the static and transfer-of-energy (hereafter denoted as TE) matrix elements contain both direct and exchange parts. The direct and exchange parts of the static and TE matrix elements can be associated with the different kinds of interionic interactions as shown in Fig. 1.

The direct part of the static term corresponds to what is usually termed the crystal field. Matrix elements for which $w = w'$ describe the shift of the free-ion energy levels due to interionic interactions. Those for which $w \neq w'$ split the free-ion terms according to the symmetry of the site, giving what are called the crystal field solutions. The exchange part of the static matrix elements split up the Kramers degenerate crystal field states when the material becomes magnetically ordered. This is known as the exchange splitting. The static matrix elements thus provide the single-ion description of the energy levels of ions in concentrated salts.

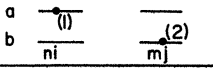
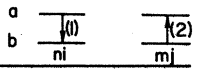
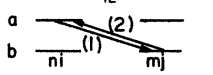
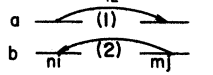
	STATIC $\langle \mu_{ni}^w \mathcal{H} \mu_{ni}^{w'} \rangle$	ENERGY TRANSFER $\langle \mu_{ni}^w \mathcal{H} \mu_{mj}^{w'} \rangle$
DIRECT	CRYSTAL FIELD $\langle a(1)b(2) \frac{e^2}{r_{12}} a(1)b(2) \rangle$ 	TRANSFER OF ENERGY VIA MULTIPOLE $\langle a(1)b(2) \frac{e^2}{r_{12}} b(1)a(2) \rangle$ 
	EXCHANGE SPLITTING $\langle a(1)b(2) \frac{e^2}{r_{12}} a(2)b(1) \rangle$ 	TRANSFER OF ENERGY VIA ELECTRON EXCHANGE $\langle a(1)b(2) \frac{e^2}{r_{12}} b(2)a(1) \rangle$ 

FIG. 1. Types of interionic Coulomb matrix elements. Single-electron orbitals are designated by a and b . The matrix elements are defined in the text.

The TE matrix elements are responsible for the delocalization of excitations and hence the exciton character of excited states. The direct part of the TE matrix elements induces a transfer of energy via the interaction of the transition moments of the electron clouds on the two interacting ions as shown in Fig. 1. Although there is no electron exchange, energy is transferred. The exchange part of the TE matrix elements produces a transfer of energy via the electron exchange, as diagrammed in the lower right-hand corner of Fig. 1. In ionic insulators this is thought to be a superexchange process, involving the intervening anions.

The matrix elements of e^2/r_{12} include the magnetic dipolar interactions, provided that the interionic interaction is solved relativistically. In practice, we usually add to the Hamiltonian terms which reproduce the relativistic effects, the most important of which look like the interaction of the magnetic moments.

If the TE matrix elements are negligible, the single-ion model, which has been the usual description of the excited states of ionic insulators, is valid. If the TE and static matrix elements are comparable in magnitude, the problem becomes intractable. If, however, the TE matrix elements are much smaller than the static matrix elements, as will be shown to be the case for RCrO_3 , then the former may be treated as a small perturbation on the latter. In this case, we first treat the single-ion ("static") problem, redescribe the crystal states as products of these single-ion eigenstates, and consider TE matrix elements among these crystal states.

Let us presume that the single-ion problem has been solved. We represent the i th ion of the n th unit cell in its ground state by g_{ni} and in an excited state

by μ_{ni}^W . Here, g and μ^W are antisymmetrized products of occupied single-electron orbitals where the orbitals are now solutions of the single-ion problem. The ground crystal state is

$$|G\rangle = |g_{01}g_{02}\cdots g_{0p}\cdots g_{ni}\cdots g_{Np}\rangle, \quad (2.4)$$

while the excited states are

$$|\mu_{ni}^W\rangle = |g_{01}g_{02}\cdots g_{0p}\cdots \mu_{ni}^W\cdots g_{Np}\rangle. \quad (2.5)$$

There are pN degenerate crystal states for each single-ion state μ^W , where W has the values 1 to V , V being the number of single-ion excited states. (The single-ion states are assumed to be nondegenerate.) To find the eigenstates of the crystal, one must solve the $(pNV+1)$ -dimensional matrix whose elements are $\langle\mu_{ni}^W|\mathcal{H}|\mu_{mj}^W\rangle$. It is easy to see that matrix elements for which $W \neq W'$ will not appreciably affect the solutions if, as we have assumed, the TE matrix elements are much smaller than the energy separations between states differing in W . As a result, the matrix breaks up into V blocks, each of dimension pN , i. e., we can treat the exciton problem for each single-ion excited state separately.

We now concentrate on the solutions of the pN -dimensional matrix of the single-ion excited state μ^W , the superscript being unnecessary in the following discussion. In order to reduce the pN -dimensional matrix to a simpler form we take linear combinations of the crystal states $|\mu_{ni}\rangle$ which transform as irreducible representations of the translation subgroup \mathcal{T} of the full space group \mathcal{G} . These are

$$|\mu_{\vec{k}}i\rangle = N^{-1/2} \sum_{n=1}^N e^{-i\vec{k}\cdot\vec{T}_n} |\mu_{ni}\rangle, \quad (2.6)$$

where \vec{T}_n is a pure lattice translation which takes a unit cell at the origin to that of n and \vec{k} is a vector in the reciprocal space. Since \vec{k} has N possible values in reciprocal space and $i=1$ to p , we still have a pN -dimensional subspace, as required. Matrix elements between states differing in \vec{k} are zero because they belong to different irreducible representations of \mathcal{T} . As a result, the matrix reduces to N p -dimensional matrices, each matrix characterized by one of the N values of \vec{k} . A typical matrix element is

$$\langle\mu_{\vec{k}}i|\mathcal{H}|\mu_{\vec{k}}j\rangle = \delta_{kk'} \sum_n e^{+i\vec{k}\cdot(\vec{T}_{ni}-\vec{T}_{nj})} \langle\mu_{ni}|\mathcal{H}|\mu_{nj}\rangle, \quad (2.7)$$

where the origin of real space is chosen as a point in the $n=1$ unit cell. In general, there will be p solutions for each value of \vec{k} . The series of solutions determine the energy dispersion and eigenvectors of the excitons as a function of \vec{k} .

B. Description of $R\text{CrO}_3$ Crystals

The materials $R\text{CrO}_3$ crystallize in an orthorhombic space group $Pbnm(D_{2h}^{16})$ ⁷ with four molecules per unit cell. A unit cell is shown in Fig. 2. As the crystals are cooled, the following typical pattern of magnetic order sets in: (i) the Cr^{+3} spins become ordered at temperature T_{N1} (282–112 °K for $R=\text{La}$ to Lu)⁸ in a predominantly antiferromagnetic structure which has, in addition, a small ferromagnetic component; (ii) the Cr^{+3} spins undergo a reorientation at temperature T_R ; (iii) the R^{+3} ions become magnetically ordered at a temperature T_{N2} , which may be accompanied by a further Cr^{+3} spin reorientation. The types of magnetic order for the Cr^{+3} and R^{+3} spins which are compatible with the crystal structure and which preserve the paramagnetic unit cell are listed in Table I. The symbols Γ_1 , Γ_2 , Γ_3 , and Γ_4 are labels for the different magnetic space groups. The symbols G , F , A , and C describe the different possible relationships among the spins on the four translationally inequivalent ions in the unit cell which are consistent with the magnetic space groups. The notation is that of Bertaut⁹ and is described at the bottom of Table I. The subscript l labels the orthorhombic crystal axis along which the Cr^{+3} spins lie. All spin configurations are antiferromagnetic except for F , which is ferromagnetic and is responsible for the small ferromagnetic component which can occur in all but Γ_1 . All studies of the $R\text{CrO}_3$ series indicate for the Cr^{+3} spins a predominantly G -type antiferromagnetic spin arrangement. We shall ignore the small canting of the spins and assume a two-sublattice antiferromagnet for describing the Cr^{+3}

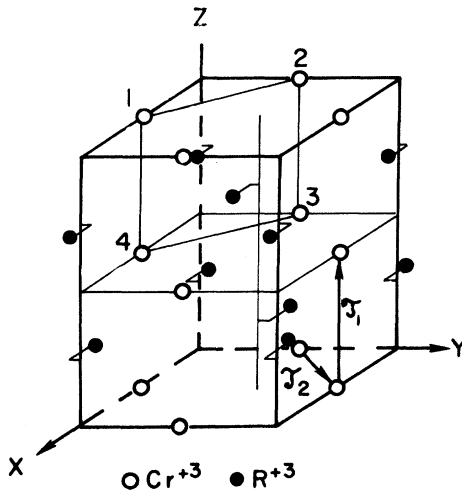


FIG. 2. Crystal structure of $R\text{CrO}_3$. The oxygens are not shown. The four translationally inequivalent Cr^{+3} ions are labeled by the numbers 1 to 4. The vectors τ_1 and τ_2 are nonprimitive lattice translations.

single-ion states. This is justifiable because the very small canting of the spins can have very little effect on the description of the single-ion states with which one begins. However, in treating the excitons which arise from each single-ion state, the full magnetic space group will be used. As a matter of convenience, we shall describe the type of magnetic order by the Cr^{+3} spin configuration G_1 , remembering that this implies all the information about the magnetic structure consistent with Table I.

The single-ion transitions which form the starting point of the analysis are the ${}^4A_2(t_{\frac{3}{2}}) \rightarrow {}^2E(t_{\frac{3}{2}})\text{Cr}^{+3}$ transitions (analog of the ruby R lines), and are indicated schematically in Fig. 2. The fourfold degeneracy of the 2E and 4A_2 states is removed completely by a combination of the low-symmetry field, spin-orbit coupling, and internal fields resulting from the magnetic order, as shown in Fig. 3. The initial and final states of the observed transitions are the lowest components of the 4A_2 and 2E manifolds, respectively. For the ground state, these are $|{}^4A_2, M_s = \frac{3}{2}\rangle$ on ions 1 and 3 ("up" sublattice) and $|{}^4A_2, M_s = -\frac{3}{2}\rangle$ on ions 2 and 4 ("down" sublattice). For the excited state, the lowest component is the $M_s = \frac{1}{2}$ (up sublattice) and $M_s = -\frac{1}{2}$ (down sublattice) spin projection of a linear combination of the two orbital basis states of $|{}^2E, M_s\rangle$. Here, and throughout this paper, the single-ion Cr^{+3} states are quantized along the direction of antiferromagnetism, $l = x, y$, or z axes for the G_1 spin configurations.

Only the optical transitions induced on the elec-

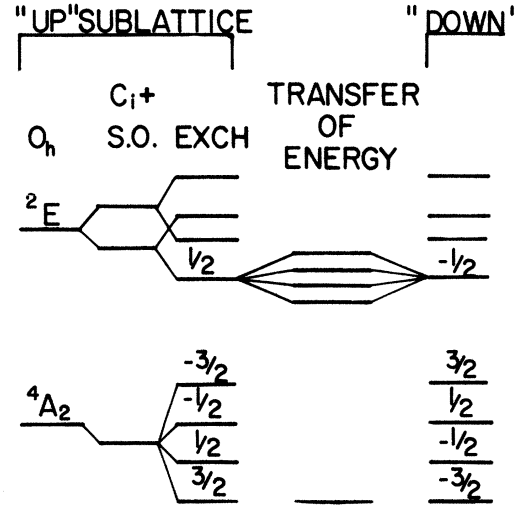


FIG. 3. Schematic energy-level diagrams for the 4A_2 ground and 2E excited states of the Cr^{+3} ions on the up and down magnetic sublattices. The effect of the low-symmetry field (C_1), spin-orbit coupling (S.O.), and exchange field (EXCH) on the eigenvectors of the octahedral field (O_h) are shown. The TE elements split each single-ion state into four $\vec{k}=0$ excitons as shown.

trons of a single ion are of concern here. Therefore, it is necessary to solve only the $\vec{k}=0$ p -dimensional matrix, since \vec{k} , which is proportional to the quasimomentum of the excitation, must be conserved in any transition. Both the ground crystal state (initial state) and the photon can be described as $\vec{k}=0$ particles, the former because the ground state contains no excitation, the latter because the wavelength of an optical photon is much greater than the interionic spacings. Therefore, only $\vec{k}=0$ excitons (final state) can be created by the action of light.

C. Solutions of $\vec{k}=0$ Matrix

The problem is very similar to that considered by Allen *et al.*⁴ in analyzing the Davydov spectrum of Cr_2O_3 . We will briefly review their analysis, adding those aspects relevant to RCrO_3 , particularly the relative intensities among the exciton transitions.

The matrix elements for the $\vec{k}=0$ matrix are

$$\langle \mu_{\vec{k}=0} i | \mathcal{H} | \mu_{\vec{k}=0} j \rangle = \sum_{n=1}^N \langle \mu_{ni} | \mathcal{H} | \mu_{nj} \rangle \equiv H_{ij}, \quad (2.8)$$

where the basis states are given by

$$| \mu_{\vec{k}=0} i \rangle = N^{-1/2} \sum_{n=1}^N | \mu_{ni} \rangle \equiv | i \rangle. \quad (2.9)$$

TABLE I. Magnetic point groups, spin representations, compatible spin configurations, and magnetic dipole selection rules to the four Davydov components corresponding to a single-ion state of Cr^{+3} in RCrO_3 . The Davydov components are labeled as in Table III.

Magnetic symmetry	Compatible spin configurations ^a	Magnetic dipole selection rules to the four Davydov components					
		Cr^{+3}	R^{+3}	ψ_1^+	ψ_1^-	ψ_2^+	ψ_2^-
$D_{2h}(D_{2h})$	$\Gamma_1 G_y, A_x, C_z$	C_z	\dots	y	z	x	
$D_{2h}(C_{2h})$	$\Gamma_2 G_z, F_x, C_y$	F_x, C_y	x	x	y, z	y, z	
	$\Gamma_3 F_y, C_x, A_z$	F_y, C_x	y	y	x, z	x, z	
	$\Gamma_4 G_x, A_y, F_z$	F_z	z	z	x, y	x, y	
<hr/>							
$A_1 \rightarrow S_{1l} = -S_{2l} = -S_{3l} = S_{4l}$		$F_1 \rightarrow S_{1l} = S_{2l} = S_{3l} = S_{4l}$					
$C_1 \rightarrow S_{1l} = S_{2l} = -S_{3l} = -S_{4l}$		$G_1 \rightarrow S_{1l} = -S_{2l} = S_{3l} = -S_{4l}$					

^aIn RCrO_3 the Cr^{+3} ions are in a predominantly G -type spin configuration.

The symbol $\mu_{\vec{k}=0}$ is unnecessary for the discussion which follows since only the $\vec{k}=0$ excitons of the lowest component of the 2E manifold are considered. Note, however, that since the single-ion eigenvectors of 2E depend on the Cr^{+3} spin configuration, the basis states $|i\rangle$ will also depend on the Cr^{+3} spin configuration. The state $|i\rangle$ must be a basis for the representation of the factor group $\mathcal{G}_{\vec{k}=0}/\mathcal{T}$, where $\mathcal{G}_{\vec{k}=0}$ is the group of the $\vec{k}=0$ vector. The generators of the $\vec{k}=0$ factor group are the operations which leave a unit cell invariant and are usually called the factor group of the crystal. When the material is magnetically ordered, it is the *magnetic* factor group which is the appropriate group. This is the group which leaves invariant both the crystallographic unit cell plus the magnetic moments on the magnetic sites. The operations of the relevant factor groups are shown in Table II. The operations of the G_y spin configuration differ from those of the paramagnetic state in that the products of $\{R|0\}$ (R is the time inversion operator) with the operations listed are not valid symmetry operations in the G_y spin configuration, whereas they are for the unordered material because the magnetic moments are flipped by $\{R|0\}$.

The effect of an external magnetic field along the direction of the Cr^{+3} spins in any of the G -type configurations is to distinguish ions 1 and 3 from 2 and 4, the spins being parallel and antiparallel to the field, respectively. This is represented by adding to the Hamiltonian \mathcal{H} the term $\mathcal{H}^{\text{mag}} = \beta \vec{H}_0 \cdot (\vec{L} + 2\vec{S})$, so that $\mathcal{H}^{\text{tot}} = \mathcal{H} + \mathcal{H}^{\text{mag}}$. Matrix elements of \mathcal{H}^{mag} in the $|i\rangle$ representation are

$$\langle i | \mathcal{H}^{\text{mag}} | j \rangle = \frac{1}{N} \sum_{n < m} \langle \mu_{ni} | \mathcal{H}^{\text{mag}} | \mu_{mj} \rangle. \quad (2.10)$$

If it is assumed that the external field does not cou-

ple states on different ions, this reduces to $\delta_{ij} \langle \mu_{ni} | \mathcal{H}^{\text{mag}} | \mu_{nj} \rangle$. By writing the basis states $|\mu_{ni}\rangle$ as in Eq. (2.5), it is easily seen that

$$H_{11}^{\text{mag}} = H_{33}^{\text{mag}} = -H_{22}^{\text{mag}} = -H_{44}^{\text{mag}} = \frac{1}{2}(g' - 3g)\beta H_0 = \bar{g}, \quad (2.11)$$

where $H_{ii}^{\text{mag}} = \langle i | \mathcal{H}^{\text{mag}} | i \rangle$ and g and g' are the g values of the ground and excited states, respectively, for an external magnetic field H_0 along the direction of antiferromagnetism.

The resulting matrix in the $|i\rangle$ representation is

$$\mathcal{H}_l^{\text{tot}} = \mathcal{H}_l + \mathcal{H}_l^{\text{mag}} = \begin{bmatrix} \bar{g}_l & H_{12}^l & H_{13}^l & H_{14}^l \\ H_{21}^l & -\bar{g}_l & H_{23}^l & H_{24}^l \\ H_{31}^l & H_{32}^l & \bar{g}_l & H_{34}^l \\ H_{41}^l & H_{42}^l & H_{43}^l & -\bar{g}_l \end{bmatrix}, \quad (2.12)$$

where l refers to the spin configuration G_l . The matrix is first simplified by using the operations of the magnetic factor group of the crystal on the matrix elements to determine relationships among the H_{ij}^l 's. In using group theory to perform these matrix simplifications, we can consider the functions $|\mu_{ni}\rangle$ rather than the actual basis states $|i\rangle$. This is because the two sets of functions have identical transformation properties under the factor-group operations. Considering the factor-group operation Θ , we find, in general, that

$$\Theta \langle \mu_{ni} | \mathcal{H} | \mu_{nj} \rangle = \langle \mu_{mi'} | \mathcal{H} | \mu_{m'j'} \rangle. \quad (2.13)$$

This implies $H_{ij} = H_{i'j'}$, since the Hamiltonian is invariant under Θ . The operations, which, in general, consist of rotations (proper and improper) and nonprimitive translations, take site ni to mi' and nj to $m'j'$ while simultaneously rotating the contours of the electronic wave functions. If Θ is anti-unitary, the complex conjugate must be taken as well. These relationships are summarized in Table III.

The resulting matrix is then diagonalized. For $\vec{H}_0 = 0$, this can be performed by a similarity transformation which reduces the representation $|i\rangle$ to that of an irreducible representation of the magnetic factor group. Wigner¹¹ has described how to find these irreducible representations (called corepresentations) for antiunitary groups. One first reduces the representations formed by the four functions $|i\rangle$, $i = 1$ to 4, in the unitary subgroup of the magnetic factor group. The characters of this representation are given by

$$\chi(\Theta) = \sum_{i=1}^4 \chi_{ni}^{s \cdot g}(\Theta), \quad \Theta \text{ in site group}$$

TABLE II. Symmetry operations of the magnetic factor groups corresponding to the Cr^{+3} spin configurations G_y , G_x , and G_z . Let C_{2x} , C_{2y} , and C_{2z} be twofold rotations through the center of a unit cell about the x , y , and z axes, respectively, and $\sigma_l = IC_{2l}$ where I is the inversion operator. R is the operation of time inversion. The translations $\vec{\tau}_1$ and $\vec{\tau}_2$ are shown in Fig. 2 and $\vec{\tau} = \vec{\tau}_1 + \vec{\tau}_2$. Products of these with $\{\vec{E}|0\}$ produce the double group. Products with $\{R|0\}$ are appropriate operations for the paramagnetic factor group only.

Cr^{+3} spin magnetic factor group	Symmetry operations of the magnetic factor group
Paramagnetic, or $G_y - D_{2h}(D_{2h})$	$\{\vec{E} \vec{0}\} \{C_{2x} \vec{\tau}_1\} \{C_{2y} \vec{\tau}\} \{C_{2z} \vec{\tau}_2\}$ $\{I \vec{0}\} \{\sigma_x \vec{\tau}_1\} \{\sigma_y \vec{\tau}\} \{\sigma_z \vec{\tau}_2\}$
$G_x - D_{2h}(C_{2h})$	$\{\vec{E} \vec{0}\} \{C_{2x}R \vec{\tau}_1\} \{C_{2y}R \vec{\tau}\} \{C_{2z} \vec{\tau}_2\}$ $\{I \vec{0}\} \{\sigma_xR \vec{\tau}_1\} \{\sigma_yR \vec{\tau}\} \{\sigma_z \vec{\tau}_2\}$
$G_z - D_{2h}(C_{2h})$	$\{\vec{E} \vec{0}\} \{C_{2z} \vec{\tau}_1\} \{C_{2y}R \vec{\tau}\} \{C_{2x}R \vec{\tau}_2\}$ $\{I \vec{0}\} \{\sigma_z \vec{\tau}_1\} \{\sigma_yR \vec{\tau}\} \{\sigma_xR \vec{\tau}_2\}$

TABLE III. Solutions of the TE matrices of the G_l ($l=x, y, z$) Cr^{+3} spin configurations. In this table, $\omega_{1l} = \exp(i\varphi_{1l})$, $\omega_{2l} = \exp(i\varphi_{2l})$, and $\omega_l^* = 1 \pm \exp(i\varphi_{1l} - i\varphi_{2l})$.

	G_y	G_z	G_x
Relationships among H_{ij}^l 's	$H_{12}^y = H_{34}^y, H_{13}^y = H_{24}^y$ $H_{14}^y = H_{23}^y$ (all real)	$H_{12}^z = H_{34}^z$ (real) $H_{13}^z = H_{24}^z, H_{14}^z = H_{23}^z$	$H_{14}^x = H_{23}^x$ (real) $H_{12}^x = H_{43}^x, H_{13}^x = H_{42}^x$
Representations ^a —unitary subgroup	$\Gamma_1^* + \Gamma_2^* = \Gamma_3^* + \Gamma_4^* - D_{2h}$	$2\Gamma_1^* + 2\Gamma_2^* - C_{2h}(x)$	$2\Gamma_1^* + 2\Gamma_2^* - C_{2h}(z)$
S_l	$\frac{1}{2} \begin{bmatrix} 1 & 1 & 1 & 1 \\ 1 & -1 & -1 & 1 \\ 1 & 1 & -1 & -1 \\ 1 & -1 & 1 & -1 \end{bmatrix}$	$2^{-1/2} \begin{bmatrix} 1 & 0 & 1 & 0 \\ 1 & 0 & -1 & 0 \\ 0 & 1 & 0 & 1 \\ 0 & 1 & 0 & -1 \end{bmatrix}$	$2^{-1/2} \begin{bmatrix} 1 & 0 & 1 & 0 \\ 0 & 1 & 0 & 1 \\ 0 & 1 & 0 & -1 \\ 1 & 0 & -1 & 0 \end{bmatrix}$
Eigenvalues of \tilde{H}_l	$E_{1l}^* = \pm H_{12}^y + H_{13}^y \pm H_{14}^y$ $E_{2l}^* = \mp H_{12}^y - H_{13}^y \pm H_{14}^y$	$H_{12}^z \pm R_{1z}$ $-H_{12}^z \pm R_{2z}$	$H_{14}^x \pm R_{1x}$ $-H_{14}^x \pm R_{2x}$
Eigenvectors ^b of \tilde{H}_l	$ \psi_{1l}^*\rangle = \frac{1}{2}(1, \pm 1, 1, \pm 1)$ $ \psi_{2l}^*\rangle = \frac{1}{2}(1, \mp 1, -1, \pm 1)$	$\frac{1}{2}(\pm 1, \pm 1, \omega_{1z}^*, \omega_{1z}^*)$ $\frac{1}{2}(\pm 1, \mp 1, \omega_{2z}^*, -\omega_{2z}^*)$	$\frac{1}{2}(\pm 1, \omega_{1x}^*, \omega_{1x}^*, \pm 1)$ $\frac{1}{2}(\pm 1, \omega_{2x}^*, -\omega_{2x}^*, \mp 1)$
$\tilde{H}_l^{\text{tot}c}$	$\begin{bmatrix} E_{1y}^* & 2 & 0 & 0 \\ 2 & E_{1y}^* & 0 & 0 \\ 0 & 0 & E_{2y}^* & 2 \\ 0 & 0 & 2 & E_{2y}^* \end{bmatrix}$	$\begin{bmatrix} E_{1z}^* & 0 & \omega_{1z}^* & -\omega_{1z}^* \\ 0 & E_{1z}^* & -\omega_{1z}^* & \omega_{1z}^* \\ (\omega_{2z}^*)^* & -(\omega_{2z}^*)^* E_{2z}^* & 0 & 0 \\ -(\omega_{2z}^*)^* & (\omega_{2z}^*)^* & 0 & E_{2z}^* \end{bmatrix}$	$\begin{bmatrix} E_{1x}^* & 0 & \omega_{1x}^* & -\omega_{1x}^* \\ 0 & E_{1x}^* & -\omega_{1x}^* & \omega_{1x}^* \\ (\omega_{2x}^*)^* & -(\omega_{2x}^*)^* E_{2x}^* & 0 & 0 \\ -(\omega_{2x}^*)^* & (\omega_{2x}^*)^* & 0 & E_{2x}^* \end{bmatrix}$

^aAs defined in Ref. 10.

^bCoefficients of the basis states $|i\rangle$ in the order $i=1, 2, 3$, and 4.

^cAll off-diagonal matrix elements are to be multiplied by $\frac{1}{4}(g' - 3g)H_0$, where $H_0 \parallel l$.

$$= 0, \quad \Theta \text{ not in site group} \quad (2.14)$$

where $\chi_{nl}^{s,s'}(\Theta)$ is the character of the representation to which μ_{nl} belongs. The resulting irreducible representations are shown in Table III. The Dimmock-Wheeler test¹² can then be used to determine whether the antiunitary operations introduce any added degeneracy. In the present case, no added degeneracy occurs. The similarity transformations S_l which perform the reduction in the unitary subgroup can be found by means of the projection operators of the appropriate irreducible representations, and are shown in Table III. The transformed energy matrices $\tilde{H} = S_l^\dagger H_l S_l$, which are not yet necessarily in diagonal form, can be diagonalized either directly or by a second similarity transformation $\tilde{H} = S_l'^\dagger \tilde{H}_l S_l'$, as described by Allen *et al.*⁴ The resulting eigenvalues and eigenvectors of the $\tilde{H}_0 = 0$ energy matrix are given in Table III. Also shown are the matrices for $\tilde{H}_0 \neq 0$ along the Cr^{+3} spin direction, given by $\tilde{H}_l^{\text{tot}} = \tilde{H}_l + S_l'^\dagger S_l^\dagger H_l^{\text{mag}} S_l S_l'$. Note that in Table III the following substitutions have been made:

$$\begin{aligned} G_z & & G_x \\ R_{1z} e^{i\varphi_{1z}} &= H_{13}^z + H_{14}^z, & R_{1x} e^{i\varphi_{1x}} &= H_{12}^x + H_{13}^x, \\ R_{2z} e^{i\varphi_{2z}} &= H_{13}^z - H_{14}^z, & R_{2x} e^{i\varphi_{2x}} &= H_{12}^x - H_{13}^x, \end{aligned} \quad (2.15)$$

$$\varphi_z = \varphi_{1z} - \varphi_{2z}, \quad \varphi_x = \varphi_{1x} - \varphi_{2x}.$$

The selection rules on the transitions to the four $\vec{k}=0$ excitons can easily be calculated assuming the transition mechanism is that of the single ion. The Cr^{+3} site symmetry C_l contains the inversion operator. Therefore, single-ion transitions within the d^3 configuration can occur only via magnetic dipole radiation, as found experimentally for RCrO_3 . For $\tilde{H}_0 = 0$, transition moments are proportional to the matrix elements $\langle G | \tilde{M} | \psi \rangle$, where ψ can be any of the four excitons ψ_{1l}^*, ψ_{2l}^* for the G_l spin configurations and $\tilde{M} = \tilde{L} + 2\tilde{S}$. Since $\langle G |$ belongs to the totally symmetric representation of the magnetic factor group \tilde{M} must transform as the same representation as ψ . The resulting selection rules can be found in Table I. Note that they are unambiguously different for each of the magnetic symmetries considered.

For G_y with $\tilde{H}_0 = 0$, only one exciton transition appears in each polarization, whereas for G_z and G_x two transitions appear in each polarization. The relative intensities of the two transitions in each polarization follow directly from the eigenvectors of the $\tilde{H}_0 = 0$ matrix with the help of some symmetry considerations on the magnetic dipole transition moments. The transition moments are expanded in the (i) representation as

$$\langle G | \tilde{M} | \psi \rangle = \sum_i C(\psi, i) \langle G | \tilde{M} | i \rangle. \quad (2.16)$$

Taking

$$\vec{M} = \sum_{ni} \vec{m}_{ni},$$

where \vec{m}_{ni} is the single-ion transition moment operator, it is seen that

$$\langle G | \vec{M} | i \rangle = N^{-1} \sum_n \langle g_{11} g_{12} \cdots g_{ni} \cdots | \vec{M} | g_{11} g_{12} \cdots \mu_{ni} \cdots \rangle = \langle g_{ni} | \vec{m}_{ni} | \mu_{ni} \rangle. \quad (2.17)$$

This is the single-ion transition moment at site ni . Relationships among the $\langle G | \vec{M} | i \rangle$ are found as was done for the H_{ij} 's, noting that \vec{M} is not invariant under the operations Θ . Denoting the ξ th component of the transition moment as $M_i^\xi = \langle G | M^\xi | i \rangle$, we find

$$\Theta M_i^\xi \equiv \Theta \langle g_{ni} | m_{ni}^\xi | \mu_{ni} \rangle = \pm \langle g_{n'j} | m_{n'j}^\xi | \mu_{n'j} \rangle \equiv \pm M_j^\xi. \quad (2.18)$$

These transition moments in terms of M_{1i}^ξ , for the G_z and G_x spin configurations, are shown in Table IV. Using these relationships and the zero-field eigenvectors of Table III, the transition moments to the four excitons can be obtained for each polarization, also shown in Table IV. The intensity ratios of the two components which appear in each polarization are shown in the last row of Table IV. Here, for instance,

$$I_i^+ / I_i^- = |\langle G | M^\xi | \psi_{1i}^+ (\psi_{2i}^+) \rangle / \langle G | M^\xi | \psi_{1i}^- (\psi_{2i}^-) \rangle|^2, \quad (2.19)$$

TABLE IV. Calculated transition moments to the crystal states and zero-field exciton states and intensity ratios of the transitions to the zero-field exciton states for the G_z and G_x Cr^{+3} spin configurations. All values except the intensity ratios are to be multiplied by M_{1z}^ξ or M_{1x}^ξ (the transition moment to $|1\rangle$) for the G_z and G_x spin configurations, respectively, where $\xi = x, y$, or z is the polarization.

$\langle G_1 M^\xi \psi \rangle$ with $\psi =$	$\xi = x$	$\xi = y$	$\xi = z$
$ 1_z\rangle (1_x\rangle)$	+1 (+1)	+1 (+1)	+1 (+1)
$ 2_z\rangle (2_x\rangle)$	+1 (-1)	-1 (+1)	-1 (+1)
$ 3_z\rangle (3_x\rangle)$	+1 (+1)	-1 (-1)	+1 (+1)
$ 4_z\rangle (4_x\rangle)$	+1 (-1)	+1 (-1)	-1 (+1)
$ \psi_{1z}^\pm\rangle$	$\pm 1 + e^{-i\varphi_{1z}}$	0	0
$ \psi_{2z}^\pm\rangle$	0	$\pm 1 - e^{-i\varphi_{2z}}$	$\pm 1 + e^{-i\varphi_{2z}}$
$ \psi_{1x}^\pm\rangle$	0	0	$\pm 1 + e^{-i\varphi_{1x}}$
$ \psi_{2x}^\pm\rangle$	$\pm 1 - e^{-i\varphi_{2x}}$	$\pm 1 + e^{-i\varphi_{2x}}$	0
$\frac{I_z^+}{I_z^-}$	$\frac{1 + \cos\varphi_{1z}}{1 - \cos\varphi_{1z}}$	$\frac{1 - \cos\varphi_{2z}}{1 + \cos\varphi_{2z}}$	$\frac{1 + \cos\varphi_{2z}}{1 - \cos\varphi_{2z}}$
$\frac{I_x^+}{I_x^-}$	$\frac{1 - \cos\varphi_{2x}}{1 + \cos\varphi_{2x}}$	$\frac{1 + \cos\varphi_{2x}}{1 - \cos\varphi_{2x}}$	$\frac{1 + \cos\varphi_{1x}}{1 - \cos\varphi_{1x}}$

the function ψ_{1z}^\pm or ψ_{2z}^\pm being appropriate according to the polarization ξ for which the moment is non-vanishing.

The relative intensities as a function of $\vec{H}_0 \neq 0$ along the Cr^{+3} spin directions follow directly from the relative intensities with $\vec{H}_0 = 0$ and the eigenvectors of \vec{H}_i^{tot} in the applied field. We have assumed that the external magnetic field which lowers the symmetry does not significantly alter the relationships among the H_{ij} 's derived for the symmetry appropriate to $\vec{H}_0 = 0$. Note that for G_y , with $\vec{H}_0 \parallel y$, the ψ_{1y}^+ and ψ_{1y}^- excitons as well as the ψ_{2y}^+ and ψ_{2y}^- excitons are mixed, as is obvious from \vec{H}_y^{tot} in Table III. Thus, the $\vec{H}_0 = 0$ forbidden transition to the ψ_{1y}^+ exciton now appears with $\vec{H} \parallel y$ and the transitions to the ψ_{2y}^+ and ψ_{2y}^- excitons each appear in both the $\vec{H} \parallel x, z$ polarizations. Here, \vec{H} is the magnetic vector of the light. For G_z and G_x with \vec{H}_0 parallel to z and x , respectively, all the excitons are mixed, and hence appear in all polarizations.

III. OBSERVATION AND ANALYSIS OF EXCITON SPECTRA

Photoelectrically determined polarized absorption curves were obtained near 7300 Å for single crystals of several of the series RCrO_3 using a 1.8-m spectrometer of the Ebert-Fastie design.¹³ The dispersing element was a 7500-line/in. grating used in the eighth order. Slits were adjusted so that a resolution of 0.25 cm⁻¹ was obtained. An EMI 9558 phototube with an S-20 surface was the sensing element. The signal was passed through an electrometer and was recorded on a logarithmic conversion recorder. An interference filter between the source and sample limited the light striking the sample to a 50-Å bandpass. At the beginning and end of a scan, calibration lines from a Fe-Ne hollow cathode lamp were superimposed on the spectra. Samples were mounted in liquid He or in a variable-temperature Dewar in which the sample was surrounded by He exchange gas. In the latter, the temperature was controlled by varying the pressure of the exchange gas in conjunction with the current of a nichrome heating resistor. The temperatures were determined from the resistance of a Ge thermistor which was mounted on the same Cu block as the sample. The temperature is accurate to better than 1.0 °K in the range 5–

15 °K. The tips of both Dewars could be placed between the poles of a Bitter magnet for obtaining external magnetic fields. Relative intensities were determined from the relative heights of the output of the logarithmic recorder, since the half-widths of the four transitions appeared equal under the same conditions of magnetic field and temperature. Absolute intensity determinations were made by measuring the area of the curves with a planimeter.

The crystals were grown by the flux evaporation technique using a PbF_2 -5-wt% B_2O_3 flux. Stoichiometric mixtures of Cr_2O_3 and R_2O_3 , comprising 15% by weight of the total material, were placed with the flux in tightly covered Pt crucibles which were maintained at 1275 °C for four days. The crystals were oriented by means of x-ray Laue backscattering photographs.

Absorption curves near 13 700 cm^{-1} for several of the RCrO_3 series at 2 °K are shown in Fig. 4. Except for $\text{ErCrO}_3\text{-}G_x$, these were obtained with no external magnetic field. These spectra can be classified into three types on the basis of their polarization characteristics. The first, exhibited by the upper ErCrO_3 trace, shows three transitions, one appearing in each polarization. The second, exemplified by HoCrO_3 , exhibits four transitions, two in the polarization $\vec{H} \parallel x$ and two in both the $\vec{H} \parallel y$ and $\vec{H} \parallel z$ polarizations. In the third case, as for instance YCrO_3 or the lower ErCrO_3 trace, four transitions appear, two with $\vec{H} \parallel z$ and two in both the $\vec{H} \parallel x$ and $\vec{H} \parallel y$ polarizations. These three types of spectra have polarization characteristics identical to those predicted for G_y , G_z , and G_x ,

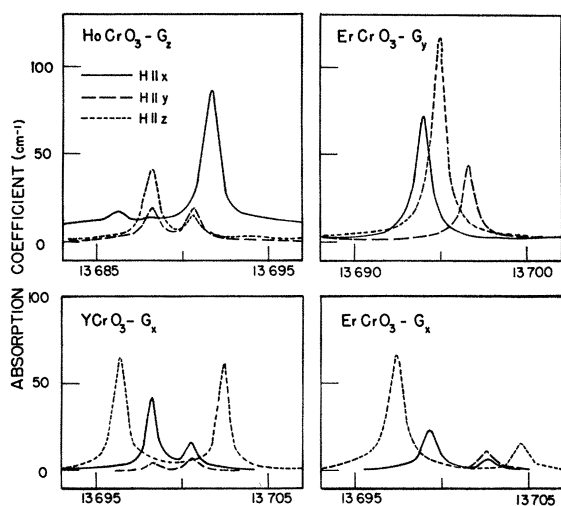


FIG. 4. Photoelectric traces of the absorption spectra of several of the RCrO_3 's at 2 °K. All were obtained with no external magnetic field except $\text{ErCrO}_3\text{-}G_x$ for which the field was $\vec{H}_0 = 12 \text{ kG}$, $\vec{H}_0 \parallel z$.

respectively (see Table I).

Neutron-diffraction measurements have been performed on some of the orthochromites, which show that most of the above conclusions about the Cr^{+3} spin configurations are correct.^{8,14,15} Thus, from the polarization of the exciton transitions the magnetic factor group may be determined. Only in the case of $\text{ErCrO}_3\text{-}G_x$ are the spectroscopic results inconsistent with those of neutron diffraction. As ErCrO_3 is warmed in zero magnetic field, the spectrum undergoes a discontinuous change at 9 °K.¹⁶ The change in the polarization of the transitions indicates a Cr^{+3} spin reorientation from G_y to G_x .

A similar change occurs at 2 °K in an external field along the z axis at 2.0 kG. Above 2 kG the spectrum remains unchanged, except for a line narrowing. Its appearance at 12 kG is shown in Fig. 4. Bertaut and Mareschal¹⁵ claim that a spin reorientation occurs at 16.8 °K and that the low-temperature phase is a mixture of G_y and G_x . Recent measurements by Holmes¹⁷ have shown, however, that at 9.8 °K an anomaly occurs in the specific heat and that simultaneously the spontaneous magnetization disappears, as indeed it must in a G_y mode, suggesting that the conclusions drawn from the spectra are correct.

A. G_y Spin Configuration - ErCrO_3 (2 °K)

ErCrO_3 is the only known example of G_y among the RCrO_3 series. The selection rules for this configuration allow observation of transitions to only three of the four excitons (two energy differences). This is not sufficient to determine the three TE matrix elements H_{ij}^y , as can be seen from the eigenvalues of \vec{H}_y in Table III. However, an external magnetic field mixes the ψ_{1y}^+ and ψ_{1y}^- excitons, allowing the ψ_{1y}^+ exciton to be observed (see Sec. IIC). Unfortunately, it cannot be observed sufficiently close to $\vec{H}_0 = 0$ to extrapolate a zero-field position. However, by comparing the calculated energies as a function of magnetic field along the y axis (eigenvalues of \vec{H}_y^{tot}) with the observed positions, one can determine the three TE matrix elements which are listed in Table V. A comparison of the calculated to the observed energy levels and relative intensities are shown in Fig. 5. In making this fit we have chosen both the position of the fourth exciton transition and the value of $\bar{g} = \frac{1}{2}(g' - 3g)\beta H_0$. Since the 4A_2 ground state contains no orbital momentum, $g = 2$. Therefore, \bar{g} determines g' , the single-ion g value of the 2E state. The calculated energies and intensities describe the observations extremely well, confirming the assumption that these transitions are the four excitons arising from a Cr^{+3} single-ion state.

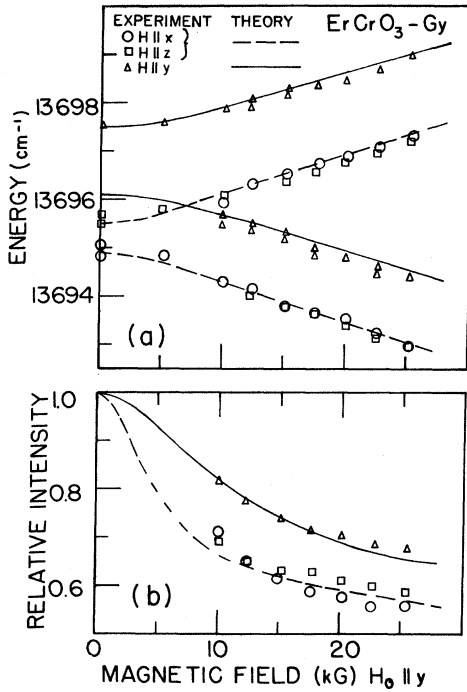


FIG. 5. Experimental and theoretical dependence of the (a) energies and (b) relative intensities among the Davydov components for each polarization as a function of magnetic field. Note that the relative intensity of only that exciton which appears at zero field is shown. That of the other exciton which appears for $\vec{H}_0 \neq 0$ is unity less the value shown. Here, $g' = 2.36$.

B. G_z Spin Configuration - HoCrO_3

The zero-field spectrum of HoCrO_3 is shown in Fig. 4. For G_z , transitions to all four excitons are allowed (see Table I). The exciton energy splittings are determined by H_{12}^z , R_{1z} , and R_{2z} . H_{12}^z is determined experimentally as half the difference between the center of gravity of the ψ_{1z}^\pm excitons ($\vec{H} \parallel x$) and the ψ_{2z}^\pm excitons ($\vec{H} \parallel y, z$). R_{1z} and R_{2z} are the moduli of $H_{13}^z + H_{14}^z$ and $H_{13}^z - H_{14}^z$, respectively, and are determined experimentally from the relations

$$R_{1z} = \frac{1}{2} \Delta E_x, \quad R_{2z} = \frac{1}{2} \Delta E_y = \frac{1}{2} \Delta E_z, \quad (3.1)$$

where ΔE_i is the zero-field splitting of the two exciton lines which appear in the $\xi = x, y$, and z polarizations. Equation (3.1) follows from Tables III and IV. Since H_{13}^z and H_{14}^z are in general complex, they cannot be determined from the zero-field splittings alone, but require a knowledge of the zero-field intensity ratios in each polarization as well. The phase angles φ_{1z} and φ_{2z} defined in Eq. (2.15) are determined experimentally from I_{1z}^+/I_{1z}^- and I_{2z}^+/I_{2z}^- , respectively, as shown in Table IV.

There is an ambiguity in the sign of φ_{1z} and φ_{2z} since the intensities depend only on the cosine of the angles. The result is four possible combinations of φ_{1z} and φ_{2z} . Two of these combinations can be eliminated by examining the spectra in an external magnetic field along the Cr^{+3} spin direction $\vec{H}_0 \parallel z$. In \vec{H}_0^{tot} (see Table III) the matrix elements depend only on the difference between the angles $\varphi_z = \varphi_{1z} - \varphi_{2z}$. Two different solutions result, one for $\varphi_z^+ = \pm(\varphi_{1z} + \varphi_{2z})$ and the other for $\varphi_z^- = \pm(\varphi_{1z} - \varphi_{2z})$. These can be distinguished by a comparison with the data. The resulting values of H_{ij}^z are shown in Table V.

The calculated intensity ratios of Table IV require that the intensity ratio I_{2z}^+/I_{2z}^- in the $\vec{H} \parallel y$ polarizations be the inverse of that in the $\vec{H} \parallel z$ polarization. This requirement is not accurately satisfied, and therefore we chose φ_{2z} to be a best fit to the intensity ratios in the two polarizations. A comparison between the calculated and observed energies and relative intensities as a function of magnetic field along the z axis is shown in Fig. 6. An excited-state g value of $g' \approx 4$ is necessary to fit the energy dependence of the transitions. This large deviation from the spin-only value is discussed in the Appendix. The calculated splittings and intensities agree fairly well with the experimental results, although the agreement is not as good as was the case for G_y . Part of the difficulty may be that the TE matrix elements are not completely independent of the external field as we have assumed. A second possible explanation may be the assumption of one isolated single-ion state. Any nearby higher-energy single-ion states also give rise to four excitons which belong to the same representations of the magnetic factor group as those of the lowest single-ion state we have been considering. Excitons from the two single-ion levels which have the same symmetry can interact, weakening the above assumption according to the size of the matrix elements and the proximity of

TABLE V. $\text{Cr}^{+3}-\text{Cr}^{+3}$ TE matrix elements for several of the $R\text{CrO}_3$ series as determined from the Davydov spectrum of the ${}^4A_2 \rightarrow {}^2E\text{Cr}^{+3}$ transitions. The matrix elements are of the form $H_{ij}^z = |H_{ij}^z| \exp(i\theta_{ij}^z)$, with $|H_{ij}^z|$ in cm^{-1} and θ_{ij}^z in degrees.

$R\text{CrO}_3-\text{Cr}^{+3}$ spin	$ H_{12}^z $	θ_{12}^z	$ H_{13}^z $	θ_{13}^z	$ H_{14}^z $	θ_{14}^z
ErCrO_3-G_y	0.5	180	0.8	0	0.2	180
HoCrO_3-G_z	0.3	180	1.7	± 44	1.0	± 8
YCrO_3-G_x	2.0	± 86	1.0	± 104	0.0	0
	1.0	± 81	2.0	± 97	0.0	0
ErCrO_3-G_x	2.2	± 107	1.7	± 157	0.1	0
	0.8	± 130	2.6	± 128	0.1	0

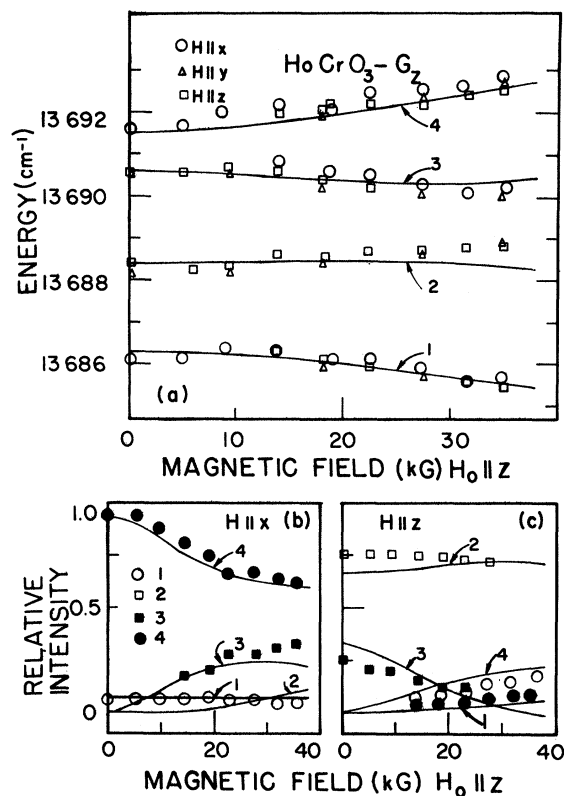


FIG. 6. Experimental and theoretical dependence of the energies and relative intensities among the Davydov components on the magnetic field $H_0 \parallel z$. The dependence of the energies is shown in (a) and those of the relative intensities in the $\vec{H} \parallel x$ and $\vec{H} \parallel z$ polarizations are described in (b) and (c), respectively. Note that the legend of (a) is different from that of (b) and (c). Here, $g' = 4.0$.

the other single-ion states. The second explanation would apply in zero magnetic field and might explain the discrepancy between the calculated and the observed intensity ratios I_{2x}^+/I_{2x}^- in the $\vec{H} \parallel y$ and $\vec{H} \parallel z$ polarizations. We have not attempted any calculations to take into account any other single-ion states, since they are not observed, and therefore no information about the resulting excitons is known. The polarization selection rules and dependence of the energy splittings and relative intensity of the transitions in an external field demonstrate that the four transitions correspond to the four Davydov-split excitons of a component of 2E .

C. G_x Spin Configuration - YCrO_3 , ErCrO_3

In Fig. 4 is shown the zero-field absorption spectrum of YCrO_3 . The polarized zero-field spectrum has been reported by van der Ziel and Van Uitert,¹⁸

while the spectrum in a magnetic field up to 20 kG has been observed by Aoyagi *et al.*⁵ The observed relative energies of the four observed excitons agree with the previously reported work within 0.2 cm^{-1} , while the center of gravity of the four exciton lines agrees within 1 cm^{-1} . Aoyagi *et al.* observe no exciton transitions in the $\vec{H} \parallel y$ polarization, in contrast to the work of van der Ziel and ourselves, where two weak lines with $\vec{H} \parallel y$ are observed. Their energies are identical to those of the $\vec{H} \parallel x$ polarization. The observed selection rules are those predicted for G_x .

Aoyagi *et al.* explained their observations using the paramagnetic factor group. They were then forced to assume two nearly degenerate single-ion levels to explain the two transitions in both the $\vec{H} \parallel x$ and $\vec{H} \parallel z$ polarizations. Allen¹⁹ has reinterpreted the experimental results of Aoyagi *et al.* taking into account the $\vec{H} \parallel y$ transitions observed by van der Ziel. Allen treats the problem using the magnetic factor group of YCrO_3 in the G_x spin configuration. He calculates that, of the four observed transitions, the lowest energy pair corresponds to the ψ_{1x}^- , ψ_{2x}^- excitons of one single-ion energy level, while the pair highest in energy corresponds to the ψ_{1x}^+ , ψ_{2x}^+ excitons of a second single-ion level. This is equivalent to setting $H_{13}^x \gg H_{12}^x$, H_{14}^x in the above discussion of the G_x spin configuration. It then follows from Eq. (2.15) that $\varphi_x \approx 180$. Allen's conclusions for YCrO_3 - G_x differ from the conclusions drawn about ErCrO_3 - G_y and HoCrO_3 - G_z in the present paper, where the four observed excitons were attributed to one single-ion state and H_{13}^x , H_{12}^x , and H_{14}^x were found to be of similar magnitudes.

We have attempted to interpret the results of Aoyagi *et al.*⁵ and some additional measurements made in this laboratory using the magnetic factor group appropriate to G_x , assuming that the four excitons arise from one low-lying single-ion level. For G_x , the analysis is similar to that of G_z . In this case

$$R_{1x} = \frac{1}{2} \Delta E_x, \quad R_{2x} = \frac{1}{2} \Delta E_x = \frac{1}{2} \Delta E_y. \quad (3.2)$$

For YCrO_3 , the intensity ratio I_{2x}^+/I_{2x}^- in the $\vec{H} \parallel x$ polarization is nearly the inverse of that in the $\vec{H} \parallel y$ polarization, as one expects using the magnetic factor group, the ratios being 0.4 and 1.75, respectively. Comparing the splitting and intensity ratios to the calculations of Sec. II C, we obtain the four possible sets of values of H_{12}^x , H_{13}^x , and H_{14}^x shown in Table V. We have measured the dependence of the transition energies and relative intensity of the excitons in three polarizations as a function of magnetic field $H_0 \parallel x$ up to 35 kG. These results are shown in Fig. 7. None of the four solutions determined from the zero-field spectra fits the observations in the magnetic field.

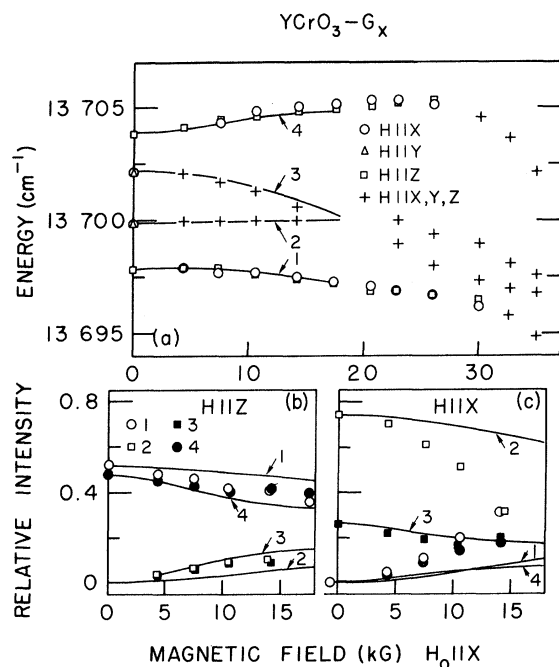


FIG. 7. Dependence of the energies and relative intensities among the Davydov components on the magnetic field $\vec{H}_0 \parallel x$ for YCrO_3 . The energy dependence is shown in (a), and the relative intensities in the $\vec{H} \parallel z$ and $\vec{H} \parallel x$ polarizations appear in (b) and (c), respectively. The curves indicate Allen's results of Ref. 19. Note that the legend of (a) differs from that of (b) and (c).

On the other hand, Allen's conclusion of two single-ion states allows one to fit the dependence of the transition energies on the field for $H_0 < 17.5$ kG, provided one allows for a shift in the center of gravity, but fails to describe the observed relative intensity dependence in the $H \parallel x, y$ polarizations, shown by the curves in Fig. 7. It therefore seems that neither description is satisfactory.

A possible explanation for the inability to explain the magnetic field dependence of the transitions is that the external field induces a Cr^{+3} spin reorientation. The spin reorientation alters the single-ion eigenstates, invalidating any description of the field dependence of the exciton states based on a fixed set of single-ion states. Both Allen and ourselves have assumed a fixed set of single-ion states. This explanation allows for both a shift of the center of gravity of the exciton transition energies as well as a dependence of the total transition intensity in each polarization on the magnetic field. The latter is observed above 20 kG and occurs because the total absorption intensity in each polarization depends directly on the square of the single-ion transition moment in that polarization. Presumably, the spin reorientation begins at low magnetic

fields.

The spectrum of $\text{ErCrO}_3\text{-}G_x$, shown in Fig. 4, is similar to that of YCrO_3 , except that one of the $\vec{H} \parallel y$ excitons is not observed. The relative intensities of the two excitons which appear in each polarization are somewhat different from those of YCrO_3 . The four combinations of TE matrix elements calculated from the spectrum of ErCrO_3 are shown in Table V. The intensity ratio I_{2x}^+/I_{2x}^- in the $\vec{H} \parallel x$ polarization is 0.25. It is therefore not surprising that ψ_{2x}^- is not observed in $\vec{H} \parallel y$ since it would be four times weaker than the already weak transition to ψ_{2x}^+ .

Above 9 °K, where the stable Cr^{+3} spin configuration in zero field is G_x , the dependence of the transition energies on a field $\vec{H}_0 \parallel x$ cannot be understood for any choice of TE matrix elements. In addition, the total absorption intensity in each polarization is strongly dependent on the field, suggesting, as for YCrO_3 , a Cr^{+3} spin reorientation induced by the field. Holmes *et al.*²⁰ have actually observed a spin reorientation for $\vec{H}_0 \parallel x$ by means of magnetization and magnetic susceptibility measurements, confirming this interpretation. They find that at 22 °K the reorientation is complete at 11 kG.

IV. COMPARISON TO Cr_2O_3

It is of interest to compare the TE matrix elements derived herein for RCrO_3 with those previously determined for Cr_2O_3 . Although the strength of the interionic interactions which lead to magnetic order for the two materials is comparable, as indicated by the similar Néel temperatures, the TE interionic interactions differ by as much as two orders of magnitude. The reason for this striking contrast lies in the different structure of the two materials and the selection rules on the relevant interionic matrix elements.

Below 308 °K, Cr_2O_3 , like RCrO_3 , is an antiferromagnet with four translationally inequivalent ions per unit cell, two with "up" spin and two with "down" spin. Allen *et al.*⁴ have shown that the five observed excitons belong to the six exciton states (two doubly degenerate) which arise from the two lowest single-ion levels of 2E . Their relative energies depend upon the single-ion splittings of the two levels and three independent TE matrix elements corresponding to the interaction of an ion with its three types of translationally inequivalent neighbors, identical to the situation of RCrO_3 . The magnitudes of the TE matrix elements are summarized in Table VI.

In order to compare the TE matrix elements in the two materials, we first assume that the major contributions to the TE matrix elements arise from nearest-neighbor (nn) interactions. We secondly assume that the superexchange is predominantly respon-

TABLE VI. Comparison of TE matrix elements and superexchange paths between Cr_2O_3 and RCrO_3 . The symbols c and z represent the number of Cr-O-Cr superexchange paths between a pair of Cr^{+3} and the number of equivalent nn pairs (ij), respectively. R_{ij} is the distance between interacting ions.

Material	(ij)	$ H_{ij} ^a$ (cm^{-1})	R_{ij} (\AA)	Cr-O-Cr angle (deg)	c	z	$\frac{ H_{ij} ^a}{ez}$ (cm^{-1})
Cr_2O_3	(12)	7.5	2.89	93	2	3	1.25
	(13)	71	3.65	133	1	6	10.8
	(14)	7.5	$\begin{cases} 2.94 \\ 2.65 \end{cases}$	$\begin{cases} 96 \\ 82 \end{cases}$	$\begin{cases} 1 \\ 3 \end{cases}$	$\begin{cases} 3 \\ 1 \end{cases}$	1.25
RCrO_3	(12)	0.8	3.79	147	1	4	0.2
	(13)	1.4	5.36	120	2	8	0.1
	(14)	0.4	3.76	144	1	2	0.2

^aWhere the values were not unambiguously determined, an average was taken. For RCrO_3 the values are averaged over the different materials and observed spin configurations.

sible for the transfer of energy. This is quite reasonable, as can be seen by extending Birgeneau's calculation of multipole interactions in ruby.²¹ Birgeneau found a maximum contribution to the TE matrix elements of $2 \times 10^{-6} \text{ cm}^{-1}$ for Cr^{+3} ions separated by 13 \AA , which resulted mainly from quadrupole-quadrupole interactions. Since the quadrupole-quadrupole interactions fall off as R^{-5} , we estimate the contribu-

tion to the H_{ij} 's in RCrO_3 to be of the order of 10^{-3} to 10^{-2} cm^{-1} . In addition, since the Cr^{+3} ion is at an inversion site in RCrO_3 , contributions to H_{ij} from dipole-dipole and dipole-quadrupole interactions will vanish.

The Cr-O-Cr superexchange paths in Cr_2O_3 involve 2.0- \AA Cr-O distances for all three types of nn. In RCrO_3 the superexchange paths are also 2.0 \AA for ions of "unlike" spin (1-2, 2-3, etc.). However, for interactions between ions of "like" spin (1-3, 2-4), the two Cr-O distances are 2.0 and about 4 \AA .²² One therefore concludes that

$$H_{13}(\text{RCrO}_3) \ll H_{13}(\text{Cr}_2\text{O}_3)$$

and

$$H_{12}, H_{14}(\text{RCrO}_3) \simeq H_{12}, H_{14}(\text{Cr}_2\text{O}_3).$$

This is in rough agreement with experiment, as seen in the last column of Table VI, where the TE matrix elements have been divided by z the number of equivalent nn and c the number of important superexchange paths.

The different superexchange paths also suggest that

$$H_{13}(\text{RCrO}_3) \ll H_{12}, H_{14}(\text{RCrO}_3),$$

whereas experimentally they are very similar (see Table VI). This can be understood by considering the spin selection rules on the TE matrix elements. For interactions between ions of like spin,

$$H_{13} = \sum_{n>m} \langle \cdots ({}^4A_2, \frac{3}{2})_{n1} \cdots ({}^2E, \frac{1}{2})_{m3} \cdots, S_z = -1 | \mathcal{H}(n1, m3) | \cdots ({}^2E, \frac{1}{2})_{n1} \cdots ({}^4A_2, \frac{3}{2})_{m3} \cdots, S_z = -1 \rangle. \quad (4.1)$$

Here, S_z is the total spin projection of the crystal state (defined along the Cr^{+3} spin direction). All other ions are in their ground state. For ions of unlike spin,

$$H_{12} = \sum_{n>m} \langle \cdots ({}^4A_2, -\frac{3}{2})_{n1} \cdots ({}^2E, \frac{1}{2})_{m2} \cdots, S_z = -1 | \mathcal{H}(n1, m2) | \cdots ({}^2E, -\frac{1}{2})_{n1} \cdots ({}^4A_2, \frac{3}{2})_{m2} \cdots, S_z = +1 \rangle. \quad (4.2)$$

Since $\mathcal{H}(ni, mj)$ is a spin-independent operator, the total spin projection must be conserved in the energy transfer. Thus, H_{12} and H_{14} are zero unless the single-ion spin projection is not a good quantum number. The above spin projections are approximately valid, although spin-orbit coupling will mix other spin states into 2E and the slight canting of the spins in RCrO_3 ²³ implies the above spin projections are not perfectly correct. Thus, the much more favorable superexchange path for H_{12} , H_{14} compared to that of H_{13} in RCrO_3 is canceled by the spin restrictions on the TE matrix elements. How-

ever, for Cr_2O_3 , $H_{13} \gg H_{12}$, H_{14} , as required by the spin selection rule because the superexchange paths are similar for interactions between ions of like and unlike spin.

The similar Néel temperatures for the two materials, in contrast to the widely differing TE matrix elements, can be understood from the different types of matrix elements responsible for the two effects. The Néel temperature is closely related to the splitting of the ground state of the ordered material. This, in contrast to the TE matrix elements, is determined predominantly by the "static"

exchange matrix elements of the form

$$\sum_{n>m} \langle \cdots ({}^4A_2, \frac{1}{2})_{ni} \cdots, S_z = -1 | \mathcal{H}(ni, mj) | \cdots ({}^4A_2, \frac{1}{2})_{nj} \cdots, S_z = -1 \rangle, \quad (4.3)$$

where all the other ions are in their ground state. The spin selection rule is satisfied regardless of whether the interacting ions are of like or unlike spin. The unfavorable superexchange path for nn ions of like spin in $RCrO_3$ will, of course, effectively eliminate contributions from these ions, but the superexchange path for nn ions of unlike spin in $RCrO_3$ should be as favorable as the nn ions in Cr_2O_3 in determining the ground-state splitting, and hence the similar Néel temperatures.

V. CONCLUSION

We have shown that the R -line spectrum of Cr^{+3} in several of the $RCrO_3$ series can be understood by treating the excitations as Frenkel excitons. These excitons must be characterized by the *magnetic* rather than the crystallographic factor group of the material in the magnetically ordered state. The symmetry operations, and hence the relationships among the TE matrix elements for different pairs of translationally inequivalent Cr^{+3} ions, are altered by the magnetic order as compared to those of the unordered state. The eigenvectors of the energy matrices belong to irreducible representations of the *magnetic* factor group, and therefore the polarization selection rules on transitions to the excitons are different from those of the unordered material. From the polarized spectra, the magnetic factor groups may be determined.

The magnetic factor groups, as determined from the spectra of $YCrO_3$ and $HoCrO_3$ at liquid-He temperatures, are consistent with the magnetic structures previously reported. However, $ErCrO_3$ is found to undergo a spin reorientation at 9°K in which the magnetic factor groups of the low and high temperature phases indicate a reorientation from a G_y to G_x spin configuration, in contrast to the results of neutron-diffraction studies.

By fitting the theory to experiment, we determined the TE energy matrix elements among the translationally inequivalent Cr^{+3} ions in $ErCrO_3-G_y$ and $HoCrO_3-G_x$. Since some of these are complex quantities, it was necessary to measure the relative intensities of the exciton transitions as well as the Davydov splittings. Furthermore, it was necessary to make these measurements as a function of an applied magnetic field along the antiferromagnetic axis of the Cr^{+3} spins. We assumed a model in which the field simply destroys the degeneracy of

the energy levels of Cr^{+3} ions on the two antiferromagnetic sublattices. For $ErCrO_3-G_x$ and $YCrO_3-G_x$, the field appears to induce a spin reorientation, and therefore they are not amenable to this model.

The resulting TE matrix elements are 5 to 100 times smaller than those of the corresponding states of Cr^{+3} in Cr_2O_3 , the only other magnetic insulator for which a Davydov splitting has been observed in the optical spectrum. We have shown that the differences can be understood qualitatively from the combined action of the different superexchange paths in the two materials and the spin selection rules on the matrix elements which describe the different interionic interaction. The result is that those TE matrix elements responsible for the large Davydov splittings in Cr_2O_3 are reduced in $RCrO_3$. However, the static type of interionic interactions, responsible for the magnetic order, are similar in the two materials. Thus, the Néel temperatures are comparable.

ACKNOWLEDGMENTS

We thank Professor H. W. Moos for his constant encouragement in this work. Many helpful discussions with John C. Wright are gratefully acknowledged.

APPENDIX

Is it reasonable for a deviation of 2 from the spin-only g value to occur for 2E ? In $Al_2O_3:Cr^{+3}$ a deviation of ± 0.4 from the spin-only value has been observed,²⁴ while for pure Cr_2O_3 the deviation is up to ± 0.85 .⁴ The octahedral field and therefore the energy-level schemes for $Al_2O_3:Cr^{+3}$ and Cr^{+3} in $RCrO_3$ are nearly identical.²⁵ For $Al_2O_3:Cr^{+3}$ the deviations were explained by second-order terms, the most favorable of which is²⁶

$$\frac{\langle {}^2E | L_x | {}^2T_1 \rangle \langle {}^2T_1 | V_{trig} | {}^2T_2 \rangle \langle {}^2T_2 | V_{trig} | {}^2E \rangle}{[W({}^2E) - W({}^2T_1)][W({}^2E) - W({}^2T_2)]},$$

where V_{trig} represents the trigonal field and W is the energy of the cubic field state. Second-order terms were necessary because the nearby states ${}^2T_1(t_2^3)$, ${}^2T_2(t_2^3)$, and ${}^4T_2(t_2^3)$ are not coupled simultaneously to 2E by either V_{trig} or V_{so} and by L_x .

This is not true for Cr^{+3} in $RCrO_3$ because the nearest state ${}^2T_1(t_2^3)$ is coupled to 2E by the low-symmetry field $V(C_4)$ and by L_x . First-order matrix elements of the form

$$\frac{\langle {}^2E | L_x | {}^2T_1 \rangle \langle {}^2T_1 | V(C_4) | {}^2E \rangle}{W({}^2E) - W({}^2T_1)}$$

are nonvanishing for Cr^{+3} in $RCrO_3$. If one chooses

the reasonable value

$$|\langle {}^2T_1 | V(C_i) | {}^2E \rangle| \simeq 200 \text{ cm}^{-1}$$

and the energy denominator to be identical to that of ruby, g' may be as large as 4 for certain choices of 2E .

*Research sponsored by the U. S. Army Research Office, Durham, N. C.

¹See, e. g., D. D. Sell, J. Appl. Phys. **39**, 1030 (1963); R. S. Meltzer, Marian Lowe, and D. S. McClure, Phys. Rev. **180**, 561 (1969).

²R. S. Meltzer, E. Cohen, and H. W. Moos, Phys. Rev. Letters **21**, 1690 (1968).

³J. P. van der Ziel, Phys. Rev. Letters **18**, 237 (1967); Phys. Rev. **161**, 483 (1967).

⁴J. W. Allen, R. M. MacFarlane, and R. L. White, Phys. Rev. **179**, 523 (1969).

⁵K. Aoyagi, K. Tsushima, and S. Sugano, Solid State Commun. **7**, 229 (1969).

⁶R. Loudon, Advan. Phys. **17**, 243 (1968).

⁷S. Quezel-Ambrunaz and M. Marechal, Bull. Soc. Franc. Mineral. Crist. **86**, 204 (1963).

⁸E. F. Bertaut, G. Bassi, G. Buisson, P. Burlet, J. Chappert, A. Delapalme, J. Mareschal, G. Roul, R. Alconard, R. Pauthenet, and J. P. Rebouillet, J. Appl. Phys. **37**, 1038 (1966).

⁹E. F. Bertaut, in *Magnetism III*, edited by G. T. Rado and H. Suhl (Academic, New York, 1963).

¹⁰G. F. Koster, J. O. Dimmock, R. G. Wheeler, and H. Statz, *Properties of the Thirty-Two Point Groups* (MIT Press, Cambridge, Mass., 1963).

¹¹E. P. Wigner, *Group Theory* (Academic, New York 1959).

¹²J. O. Dimmock and R. G. Wheeler, in *The Mathematics of Physics and Chemistry*, edited by H. Margenau and G. M. Murphy (Van Nostrand, Princeton, N. J., 1964), Vol. 2, Chap. 12.

¹³W. G. Fastie, H. M. Crosswhite, and P. Gloersen, J. Opt. Soc. Am. **48**, 106 (1958).

¹⁴E. F. Bertaut, G. Buisson, A. Delapalme, B. Van Laar, R. Lemaire, J. Mareschal, G. Roul, J. Schweitzer, Vu Van Qui, H. Bartholin, M. Mercier, and R. Pauthenet, in *Proceedings of the International Conference on Magnetism, Nottingham*, 1964 (The Institute of Physics and the Physical Society, London, 1965), p. 275.

¹⁵E. F. Bertaut and J. Mareschal, Solid State Commun. **5**, 93 (1967).

¹⁶R. S. Meltzer and H. W. Moos, J. Appl. Phys. **41**, 1240 (1970).

¹⁷L. M. Holmes (private communication).

¹⁸J. P. van der Ziel and L. G. Van Uitert, Phys. Rev. **179**, 343 (1969).

¹⁹J. W. Allen, Solid State Commun. **8**, 53 (1970).

²⁰L. Holmes, M. Eibschutz, and L. G. Van Uitert, J. Appl. Phys. **41**, 1184 (1970).

²¹R. J. Birgeneau, J. Chem. Phys. **50**, 4282 (1969).

²²The larger Cr-O distances for the eight nn of like spin vary between 3.7 and 4.8 Å.

²³In Ref. 20 this has been shown to be 2° for ErCrO₃.

²⁴S. Sugano and I. Tsujikawa, J. Phys. Soc. Japan **13**, 899 (1958).

²⁵The evidence for this is (1) the similarity of the overall optical absorption spectra and (2) the nearly identical Cr-O bond distances and approximately octahedral environment created by the six oxygens nearest a Cr⁺³ ion in the two materials.

²⁶S. Sugano and Y. Tanabe, J. Phys. Soc. Japan **13**, 880 (1958).

Magnetic Relaxation in an Exactly Soluble Model

J. A. Tjon*

Institute for Theoretical Physics, State University of New York, Stony Brook, New York 11790

(Received 16 April 1970)

Some nonequilibrium properties of an impurity in a linear chain of spins with nearest-neighbor interaction of the isotropic X - Y type are studied. It is shown that under certain conditions its behavior is in agreement with the general principles of statistical mechanics. The relaxation in the presence of a transverse field is also studied, and it is found that in the weak coupling region the approach to equilibrium is described by a sum of exponentials. However, the results do not agree with the solution of the Bloch equations.

I. INTRODUCTION

The magnetic relaxation in a spin system which is isolated from the lattice vibrations has been the subject of interest in the past years.¹⁻³ In the the-

oretical considerations, one normally assumes that the methods which are employed in nonequilibrium statistical mechanics also apply in this situation. On the other hand, it was recently demonstrated that a nontrivial model such as the X - Y